ACADEMIC PRESS

Available online at www.sciencedirect.com

SCIENCE DIRECT®

DEVELOPMENTAL BIOLOGY

Developmental Biology 264 (2003) 64–76

www.elsevier.com/locate/ydbio

Radiographic analysis of zebrafish skeletal defects

Shannon Fisher,[a,*,1] Pudur Jagadeeswaran,[b] and Marnie E. Halpern[a]

[a] *Department of Embryology, Carnegie Institution of Washington, Baltimore, MD 21210, USA*

[b] *Department of Cellular and Structural Biology, University of Texas Health Science Center, 7703 Floyd Curl Drive, San Antonio TX 78284, USA*

Received for publication 11 February 2003, revised 18 June 2003, accepted 18 June 2003

Abstract

Systematic identification of skeletal dysplasias in model vertebrates provides insight into the pathogenesis of human skeletal disorders and can aid in the identification of orthologous human genes. We are undertaking a mutagenesis screen for skeletal dysplasias in adult zebrafish, using radiography to detect abnormalities in skeletal anatomy and bone morphology. We have isolated *chihuahua*, a dominant mutation causing a general defect in bone growth. Heterozygous *chihuahua* fish have phenotypic similarities to human osteogenesis imperfecta, a skeletal dysplasia caused by mutations in the type I collagen genes. Mapping and molecular characterization of the *chihuahua* mutation indicates that the defect resides in the gene encoding the collagen I(α1) chain. Thus, *chihuahua* accurately models osteogenesis imperfecta at the biologic and molecular levels, and will prove an important resource for studies on the disease pathophysiology. Radiography is a practical screening tool to detect subtle skeletal abnormalities in the adult zebrafish. The identification of *chihuahua* demonstrates that mutant phenotypes analogous to human skeletal dysplasias will be discovered.

Keywords: Zebrafish; X-ray; Osteogenesis imperfecta; Collagen

Introduction

A wide range of developmental events culminates in the final structure and morphology of the adult skeleton. This is evidenced by the variety of genes that are mutated in human skeletal dysplasias. Mutations affecting the earliest patterning events, such as somite segmentation, lead to abnormalities in the adult vertebral column (Li et al., 1997). Mutations of transcription factors (el Ghouzzi et al., 1997; Jabs et al., 1993; Lee et al., 1997; Mundlos et al., 1997) or components of extracellular signaling pathways (Gong et al., 1999; Vajo et al., 2000) affect later events of cell differentiation and proliferation, sometimes producing widespread defects in bone growth and maturation. Mutations in components of cartilage or bone matrix also have profound effects on the development of the skeleton (Francomano et al., 1996) and on its response to injury or stress. Despite significant advances, many genes responsible for skeletal abnormalities in humans have not yet been identified.

Mutations of homologous mouse genes often mirror the phenotypes of human skeletal dysplasias and help reveal the underlying mechanisms of the disease process (Bonadio et al., 1990; Brunet et al., 1998; Chipman et al., 1993; Khillan et al., 1991; Komori et al., 1997; Otto et al., 1997; Pereira et al., 1993). In fact, the prior discovery of a mouse mutant has sometimes aided in identification of the corresponding human gene (Brunet et al., 1998; Satokata and Maas, 1994). Models for human disorders have been created by targeted mutagenesis in the mouse. However, while it is straightforward to create null mutations in mouse genes, it is more complicated to generate specific point mutations. Since many human skeletal dysplasias are caused by missense mutations, they can best be accurately modeled by similar alleles in other organisms. Systematic screens for point mutations have recently been undertaken in the mouse, and in their first phase are yielding promising collections of dominant mutations (Hrabe de Angelies et al., 2000; Nolan et al., 2000). However, mutagenesis screens in the mouse

* Corresponding author. Fax: +1-410-955-7427.

E-mail address: sfisher4@jhmi.edu (S. Fisher).

[1] Current address: Institute of Genetic Medicine, Johns Hopkins University School of Medicine, Baltimore, MD 21287, USA.

0012-1606/$ – see front matter © 2003 Elsevier Inc. All rights reserved.
doi:10.1016/S0012-1606(03)00399-3

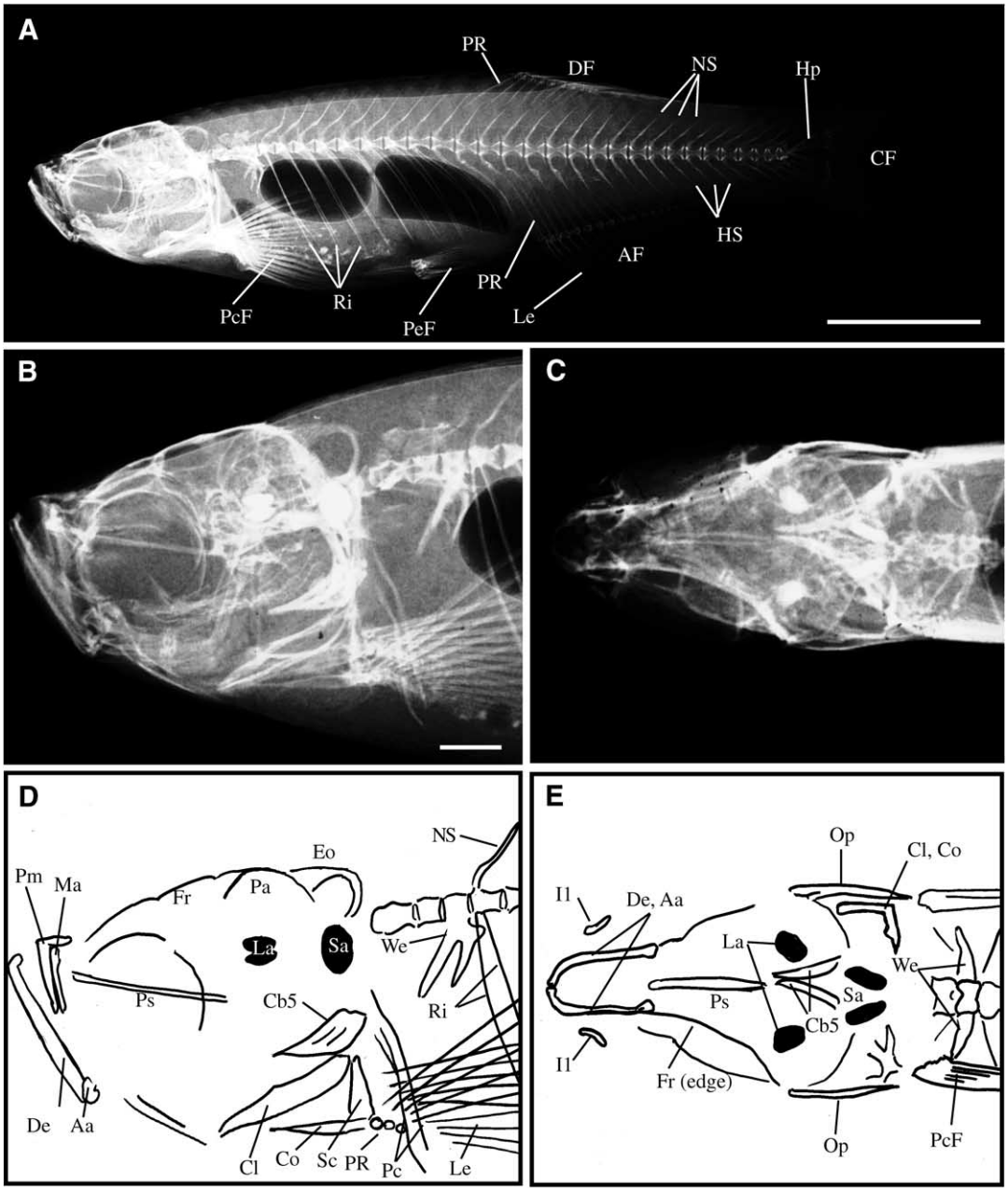

Fig. 1. Radiography reveals detailed skeletal anatomy of adult zebrafish. (A) Side view of a WT with features of the skeleton indicated (see below for key to abbreviations). (B) A higher magnification of the cranial skeleton. (C) Dorsal view of the cranial skeleton. (D) Line drawing corresponding to the radiograph in (B). (E) Line drawing corresponding to the radiograph in (C). Scale bars are 5 mm in (A) and 1 mm in (B–E). Abbreviations: Aa, anguloarticular; AF, anal fin; Cb5, fifth ceratobranchial arch, with pharyngeal teeth; CF, Caudal fin; Cl, cleithrum; Co, corocoid; Do, dentary; DF, dorsal fin; Eo, exoccipital; Fr, frontal; HS, hemal (ventral) spine; Hp, hypurals of caudal fin; I1, infraorbital 1; Io, interopercle; La, lapillus (otolith); Le, lepidotrichia (membranous bones of fin skeleton); Ma, maxilla; NS, neural (dorsal) spine; Op, opercule; Pa, parietal; Pc, postcleithrum; PcF, pectoral fins; PeF, pelvic fins; Pm, premaxilla; PR, proximal radials (pterygiophores) of anal and dorsal fin skeletons; Ps, parasphenoid; Ri, ribs; Sa, sagitta (otolith); Sc, scapula; We, Weberian apparatus.

present significant barriers of cost and labor, and are presently limited to large, multilab consortia.

Large-scale screens for mutations disrupting vertebrate embryogenesis have been carried out in the zebrafish *Danio rerio* (Driever et al., 1996; Haffter et al., 1996a). The zebrafish is amenable to this approach for several reasons, including a short generation time, reliable mutagenesis techniques, and large numbers of accessible, optically clear embryos. It is the ability to observe early development, and identify morphological abnormalities using a low magnification stereomicroscope, that has made screening for early-acting mutations so productive in the zebrafish. Features

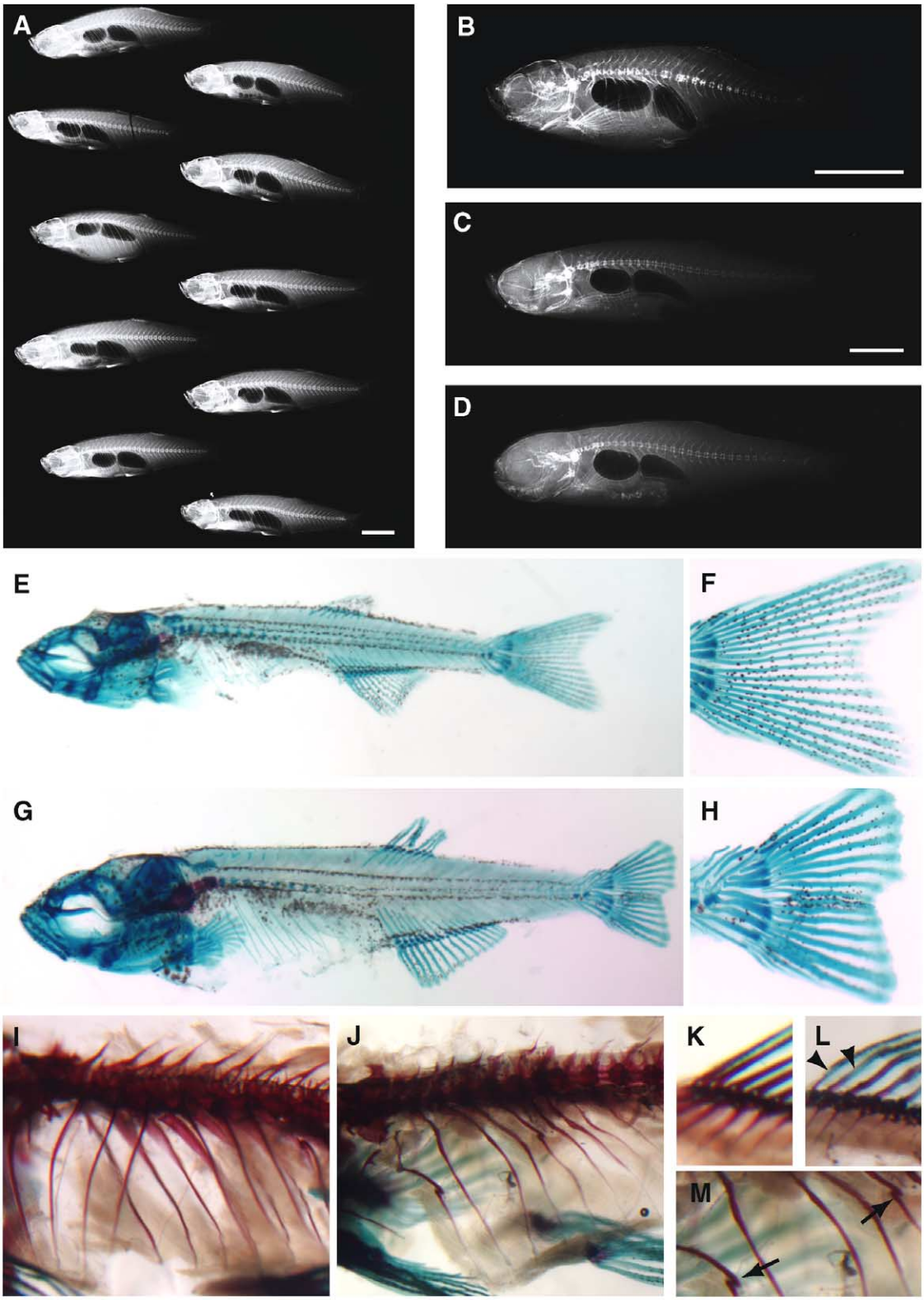

Fig. 2. Characterization of the dominant skeletal mutation *chihuahua*. (A) Example of a screening radiograph of 10 adult fish. (B) Radiograph of *chi*/+ fish, taken at approximately 10 months of age. (C, D) WT (C) and heterozygous mutant (D) progeny of *chi*/+ fish; radiographs taken at 4 weeks of age. (E–H) Alcian blue/alizarin red skeletal staining of wild-type (E, F) and *chi*/+ (G, H) fish at 4 weeks. Note especially the shorter, thicker lepidotrichia in the tail fin of the *chi*/+ fish (H), compared with WT (F). (I–M) Alcian blue/alizarin red staining of WT (I, K) and *chi*/+ (J, L, M) fish at 4 months. Arrowheads in (L) indicate areas of uneven mineralization, seen as gaps in alizarin red staining, in the dorsal fin lepidotrichia of the *chi*/+ fish (comparable view of WT fish shown in K). Arrows in (M) indicate broken and rehealed ribs in the *chi*/+ fish. Scale bars are 5 mm in (A) 5 mm in (B), and 1 mm in (C) and (D).

that develop later, after the larvae begin feeding, have been less well studied.

Descriptive studies of zebrafish skeletal development have also focused on early events (Cubbage and Mabee, 1996; Morin-Kensicki and Eisen, 1997; Morin-Kensicki et al., 2002; Schilling and Kimmel, 1994), and in general are consistent with observations for other vertebrates. Mutations have been found in previous genetic screens that affect the development of the skeleton, particularly the cartilages of the skull (Neuhauss et al., 1996; Piotrowski et al., 1996; Schilling et al., 1996). Both lineage analysis and mutant characterization have revealed similarities in the development of the chondrocranium (reviewed in Schilling, 1997). However, complete maturation of the skeleton is a relatively late event in zebrafish development, and juvenile fish are fully mobile and sexually mature before the skeleton is fully mineralized. Most of the identified mutations are homozygous embryonic lethal, and it is impossible to study their effects on later events in skeletal development.

Traditional histological methods, such as alcian blue/alizarin red staining, have been used effectively to describe skeletogenesis in the zebrafish (Cubbage and Mabee, 1996). However, they are time consuming and, for the purposes of mutational screens, have the disadvantage of requiring sacrifice of the animals. We have devised a radiographic method to overcome these disadvantages and used it to examine adult zebrafish for dominant mutations affecting the skeleton.

A few zebrafish mutations that affect somite segmentation are viable and later show defects in the adult vertebral column (van Eeden et al., 1996). This suggests that it will be possible to find additional viable mutants, with defects in later processes and with more subtle phenotypes, through screens targeted specifically at skeletal mutants. Radiography is a practical and powerful method for detecting subtle skeletal abnormalities and can be incorporated into a genetic screen. We describe the recovery and characterization of *chihuahua (chi),* a dominant mutation causing a general defect in bone growth and maturation. We show that a molecular lesion in a zebrafish type I collagen gene is associated with the *chi* mutant phenotype, demonstrating that *chi* is a useful model for the human skeletal dysplasia osteogenesis imperfecta (OI), and that mutagenesis screens in zebrafish are likely to yield skeletal dysplasias similar to human disorders.

Materials and methods

Care and maintenance of fish

Zebrafish *Danio rerio* were raised and maintained according to standard protocols (Westerfield, 1995). The mutant allele *chihuahua*^{dc124} was maintained by intercrosses of heterozygous parents or outcrosses to wild-type fish.

Radiography

For radiography, fish were lightly anesthetized with MESAB as described (Westerfield, 1995). Radiography was performed in a Faxitron MX-20 cabinet X-ray machine, for 3–4 s at 17–20 kVolts, with three-to five fold magnification. High resolution Min-R 2000 film and intensifying screens (Kodak) were used. For assignment of bones in radiographs, comparison was made to stained, dissected skeletal preparations; Cubbage and Mabee (1996) was used as a reference for identification of skull bones.

Mutagenesis

Ethyl nitrosourea (ENU) mutagenesis was performed by using the AB wild-type background (Streisinger et al., 1981), essentially as described (Mullins et al., 1994). Adult males were treated with ENU at a concentration of 3 mM in fish water, for 1 h at 21°C. Treatment was repeated at 2- to 3-day intervals for a total of three treatments. Males were allowed to recover for at least 4 weeks, giving time for mutagenized postmeiotic sperm to be cleared from the reproductive system. They were then mated with AB females to produce the F_1 generation, which was screened for dominant phenotypes. Fish showing skeletal abnormalities were mated naturally, or sperm and eggs were expelled for in vitro fertilization (Westerfield, 1995). Confirmation of the dominant mutant phenotype was obtained by screening the adult progeny.

Skeletal staining

Alcian blue/alizarin red staining was performed as previously described (Fisher and Halpern, 1999). Briefly, fish are fixed overnight in 4% paraformaldehyde/PBS, then stained overnight in 0.1% alcian blue in methanol/glacial acetic acid (7:3). After gradual rehydration, soft tissues are removed by trypsin digestion. Following staining in alizarin red (0.05% in 1% KOH), specimens are cleared by gradual transfer into glycerol.

In situ hybridization

Partial cDNA clones of type I collagen genes were identified among zebrafish expressed sequence tags (ESTs) by BLAST homology search; clone fa99c12 is *colla1,* and clone fa99d08 is *colla2.* Clones were obtained from Research Genetics (Huntsville, AL), and digoxigenin-labeled antisense RNA probes were transcribed with T7. For larvae up to 3 days, whole-mount in situ hybridizations were performed essentially as described (Fisher et al., 1997). For older fish, in situ hybridizations were performed on sec-

tioned tissue. Frozen sections were cut of paraformaldehyde fixed specimens, mounted on glass slides, and dried at room temperature. After a brief prehybridization, sections were hybridized with digoxygenin-labeled probe overnight in a sealed container. After high stringency washes, the slides were incubated with diluted anti-digoxygenin antibody conjugated to alkaline phosphatase (Roche). Staining for alkaline phosphatase activity was carried out as for whole-mount in situ hybridizations.

Radiation hybrid mapping of collagen genes

DNA from a zebrafish-mouse radiation hybrid panel was used as previously described (Hukriede et al., 1999) to localize *colla1* and *colla2* on the zebrafish map. Primers for *colla1* were CAGACTCCACCTGCTTATTCTACAC (forward) and TTGACATCGCCCCTATGGACGTTG (reverse), and for *colla2,* CATGAGGTAGTTTAAACCTTACGG (forward) and GGACATTGGCCCAGTCTGTTTCAA (reverse). Data were analyzed online, using an interactive mapping program (http://mgchd1.nichd.nih.gov:8000/zfrh/beta.cgi).

Meiotic mapping of chi

Fish carrying the *chi* mutation on the original AB background were mated to fish of the WIK background to make the polymorphic mapping cross. The female *chi*/+ progeny were used to generate haploid embryos (Westerfield, 1995). At 5 days, genomic DNA was prepared from individual wild-type and mutant haploid embryos; bulked segregant analysis and mapping were performed as described (Postlethwait et al., 1994), using simple sequence length polymorphism (SSLP) markers (Knapik et al., 1996). To map *colla1,* amplification was performed with the primers TCGGCACGAGAGAACTGGTACACA (forward) and TCCTGATTAGGTGCACCAACGTCC (reverse), and the product digested with *Rsa*I.

Cloning and sequence analysis of colla1

The EST clone of *colla1* was used as a probe to identify additional clones from a cDNA library of adult zebrafish fin (gift of Steve Johnson). Analysis of these clones and assembly of a contiguous sequence yielded a total 3.7 kb of sequence, encoding a protein corresponding to the last 841 of the 1464 residues of the mammalian protein. To identify the remaining sequence, the zebrafish translated genomic database was searched for homology to the trout Colla1 N-terminus. The putative first exon was placed on the radiation hybrid panel to confirm its identity, and RT-PCR was used to clone and sequence the remaining *colla1* cDNA. The sequence of zebrafish *colla1* is available under GenBank Accession no. AY380817.

Identification of chi^{dc124} mutation

For sequence analysis of *colla1* in *chi,* RNA was isolated from a *chi*/+ adult. Reverse transcription PCR (RT-PCR) was performed to amplify the entire coding sequence in overlapping fragments, and the amplification products were directly sequenced. After identification of the mutation, the mutation was confirmed by sequence analysis of RNA from pools of *chi*/+ and *chi/chi* embryos. As further confirmation of the lesion in *chi,* RNA or genomic DNA was isolated from individual WT, *chi*/+, and *chi/chi* embryos and WT and *chi*/+ adults. The resulting cDNA or gDNA was amplified with primers flanking the mutation and digested with *Bst*F5I, which cuts the mutated but not the WT sequence.

Results

Radiography of normal adult fish

Through the use of an X-ray machine designed for small specimen radiography, we obtained much higher resolution radiographs than possible with standard clinical equipment. The relatively low energy X-ray tube (1–35 kV) affords greater contrast in soft tissues that lack a high degree of calcification, and the small focal spot of the X-ray beam (20 μm) minimizes the scatter typically associated with magnification of radiographs. Standard X-ray film can be used (e.g., X-Omat), but greater detail and a shorter exposure time can be achieved through the use of single-sided, fine grain emulsion film with the appropriate intensifier screen, such as MinR-2000 (Kodak). The threefold magnification generally used also allows resolution of fine structures and detection of subtle defects.

As a necessary prerequisite for mutagenesis screens, we established a base of knowledge about adult zebrafish skeletal morphology that can be detected radiographically. The postcranial skeleton of the zebrafish is simple compared with that of tetrapods, and with a single side view radiograph it is possible to identify most of the bones (Fig. 1A). The number of vertebrae is variable (average is 30.3 ± 0.5; $n = 30$), and they fall into 3 categories. The first 4 vertebrae are specialized and serve as attachments for the Weberian apparatus, which transduces vibrations from the gas-filled swim bladder to the inner ear. There are 10 or 11 rib-bearing trunk vertebrae, followed by 16 or 17 tail vertebrae, each with a ventral hemal arch and spinous process. All vertebrae have a dorsal neural arch and spinous process. There are 3 midline fins (dorsal, tail, and anal), and 2 sets of paired fins (pectoral and pelvic) which correlate with the fore- and hindlimbs of tetrapods (van der Hoeven et al., 1996). The slender membranous bones of the external fins, the lepidotrichia, have no direct correlate in the tetrapod skeleton.

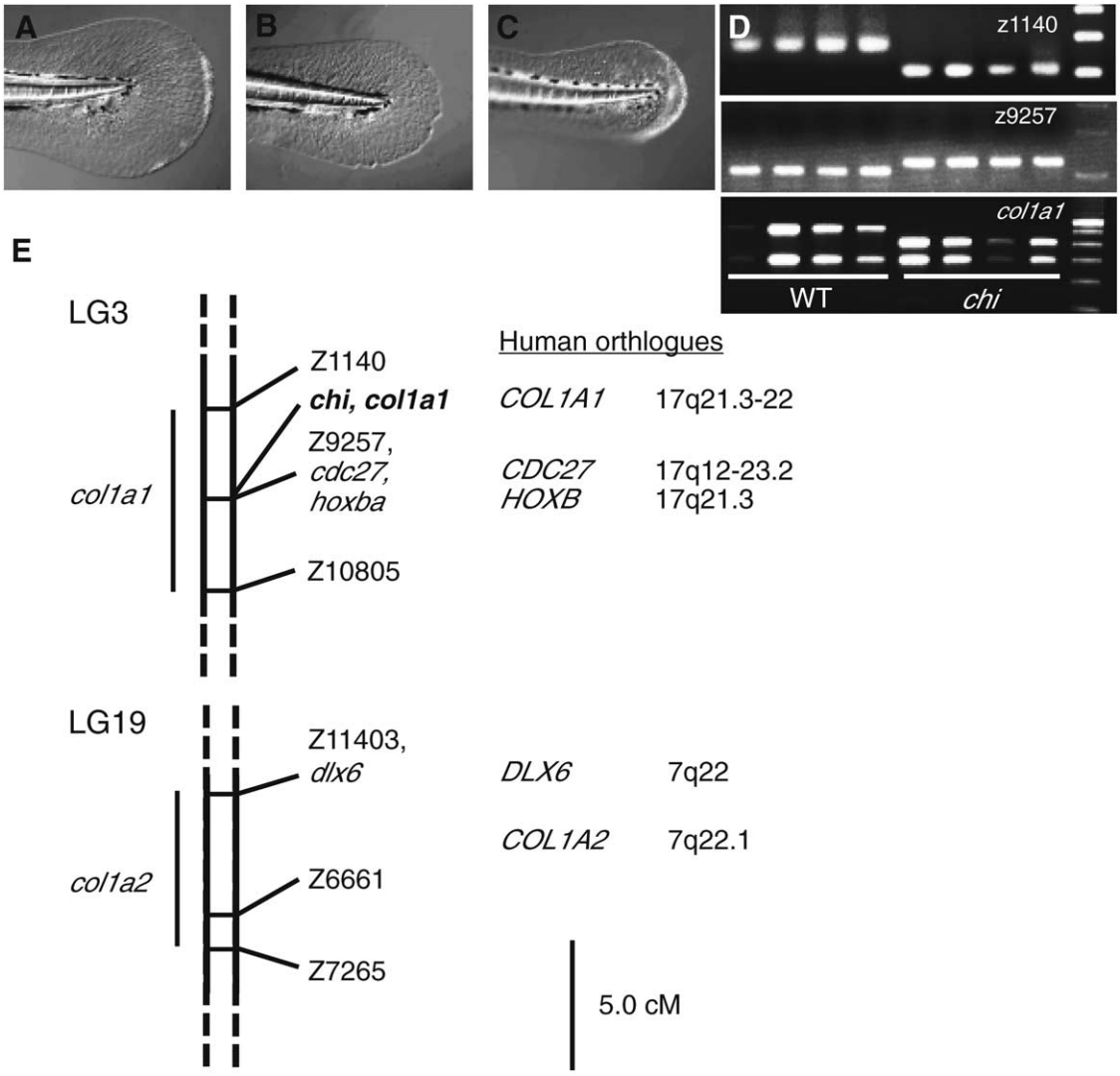

Fig. 3. Mapping of the *chi* mutation and zebrafish *colla1* and *colla2* genes. (A–C) Caudal fin folds of WT (A) and *chi*/+ (B, C) larvae at 10 days. Fin folds of *chi*/+ larvae are narrower (B), and sometimes curve sideways (C). (D) Haploid embryos from a *chi* mapping cross were sorted by caudal fin fold as WT or mutant, and genomic DNA from individual embryos subjected to PCR for SSLP markers on LG 3. In the top panel, the Z1140 primers amplified the WIK-specific fragment (~190 bp) from four WT samples, and the AB-specific fragment (~105 bp) from four *chi* samples. In the second panel, the Z9257 primers amplified the WIK-specific fragment (~600 bp) from the same four WT samples, and the AB-specific fragment (~700 bp) from the *chi* samples. In the third panel, digestion with *Rsa*I after amplification of a *colla1* fragment yields an upper band of ~400 bp in the WT samples and ~300 bp in the *chi* samples. The last lane in each panel contains molecular weight markers (100 bp ladder; Life Technologies). (E) Maps of portions of LG3 and LG19, with the positions of *colla1*, *chi*, and *colla2* indicated. Both collagen genes were mapped on a mouse–zebrafish radiation hybrid panel (Hukriede et al., 1999), using primers derived from the public EST entries. The intervals of their positions are indicated by the vertical lines to the left of each map. In each case, the regions represent blocks of conserved synteny with the human genome, as indicated by the adjacent map positions of the human orthologues. The scale of the maps and relative marker positions are taken from the SSLP reference map (http://zebrafish.mgh.harvard.edu/mapping/ssr map index.html).

The anatomy of the skull is considerably more complicated. While some bones cannot be clearly distinguished, it is possible to identify many major features in the side view (Fig. 1B) and the dorsal view (Fig. 1C). The most prominent features of the skull radiographs are the otoliths; they serve as easy reference points in the caudal skull in both the side and dorsal views. The lower jaw, comprised of the dentary and anguloarticular bones, is prominent in both views. In the side view, the premaxilla and maxilla of the upper jaw, and the upper edge of the orbit, can be easily seen.

The parasphenoid is clearly seen in the side view passing diagonally behind the orbit, indicating the bottom edge of the brain case, and is outlined by radiodense lines near the midline in the dorsal view. The membranous bones in the vault of the skull are outlined along their top edge by a radiodense line in the side view. More caudally, the fifth ceratobranchials are particularly prominent in both views, although the phanyngeal teeth on them cannot be easily resolved.

Although the clearest images are obtained from fish with

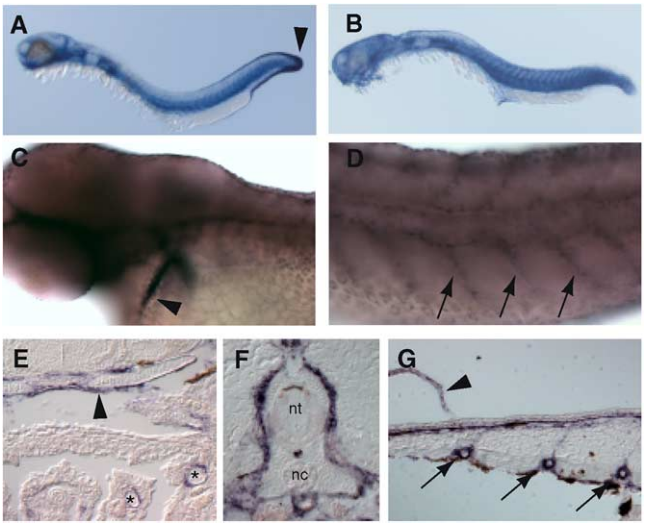

Fig. 4. Expression of collagen genes in ectoderm and developing skeletal structures. (A, B) Whole-mount *in situ* hybridization of *colla1* (A) and *colla2* (B) in 1-day-old embryos. Both genes are expressed in surface ectoderm, but only *colla1* shows strong labeling in the caudal fin fold (arrowhead in A). (C, D) Whole-mount in situ hybridization of *colla1* in 3-day larva, showing expression in the cleithrum (arrowhead in C) and (D) in cells surrounding the notocord and between the myotomes (arrows), in the developing vertebral column. (E–G) *In situ* hybridization of *colla1* on sections of fish at 6 weeks. (E) *colla1* is expressed in cells surrounding the cartilage of the basal plate (arrowhead in E) and branchiostigal rays (asterisks in E) in the chondrocranium. (F) In the developing vertebral column, *colla1* is expressed by cells surrounding the cartilage of the neural arch and vertebral body, but not in the cartilages themselves; positions of the neural tube (nt) and notochord (nc) are indicated. (G) Strong *colla1* expression is seen in the ribs (arrows), and also in the pectoral fin (arrowhead). (A–D) are side views with anterior to the left; (E) and (F) are transverse sections; and (G) is a coronal section with anterior to the left.

well mineralized skeletons (approximately 2 months and older), it is possible to glean useful information from imaging fish as young as 1 month (see Fig. 2C and D). In these cases, it is necessary to decrease the energy of the X-ray tube to 16–17 kV.

There is some variability in skeletal structures of wild-type fish, and a low incidence of abnormalities (<2%). The etiologies of these are unknown, but likely include nutritional factors, exposure to chemicals, and disease. When screening for mutations, some of the fish saved as potential mutants will have a nongenetic cause underlying their abnormalities. These fish will be distinguished from genuine carriers of mutations by their failure to transmit the phenotype to their progeny.

Screening for new skeletal mutants

To screen for new mutations that affect skeletal patterning, we devised an efficient method for obtaining radiographs of large numbers of fish. Adult fish are lightly anesthetized in groups of 10 and laid out on the removable supporting platform of the X-ray machine. After the radiograph is taken (Fig. 2A), the fish are placed in individual beakers of water. They revive and can remain there for several hours, until the films have been developed and analyzed.

In a pilot screen to assess the feasibility of this approach, we examined 2000 F_1 fish, heterozygous carriers of ENU-induced mutations, to identify potential dominant skeletal dysplasias. We used a combination of visual inspection and X-rays, either as the primary screen or as confirmation of suspected defects. Approximately 15 fish were saved as potential mutants, and 8 successfully outcrossed for confirmation. Most of these fish failed to produce affected progeny, indicating that their skeletal abnormalities did not have a genetic basis. We identified and recovered 1 mutation, *chihuahua*^{dc124} *(chi);* the heterozygous founder transmitted the mutant phenotype to 42% of its progeny (n = 107), consistent with a dominant mutation.

Chihuahua: model of human osteogenesis imperfecta

While adult *chi*/+ fish can be recognized as approximately 20% shorter than age-matched wild-type fish, their outward appearance gives no indication of their widespread skeletal dysplasia (Fig. 2B). When examined radiographically, all bones appear to be misshapen and show more irregular radiodensity than in WT. Radiographs demonstrate this phenotype as early as 1 month of age (Fig. 2D).

We examined earlier stages of skeletal development in *chi*/+ fish by histological staining. At early larval stages, when the skeleton is largely cartilagenous, *chi*/+ fish appear indistinguishable from their WT siblings (data not shown). At approximately 1 month, the caudal fins are noticeably abnormal in *chi*/+ fish; the lepidotrichia, the longitudinal, membranous bones of the fins, are thickened and shorter than in wild-type siblings (Fig. 2G and H). In young adult *chi*/+ fish, bone growth and mineralization are both abnormal. Vertebrae are irregular with short dorsal spinous processes (Fig. 2J), and areas of uneven mineralization are found in many bones (arrowheads in Fig. 2L). Also apparent are breaks in the ribs, which have healed with prominent callus formation (arrows in Fig. 2M). Overall, the phenotype had characteristics similar to human OI, including bone growth disturbances, uneven mineralization, and apparent bone weakness. Both OI and *chi* are also dominant genetic disorders.

The abnormal caudal fin growth in *chi*/+ fish at 1 month prompted us to examine tail growth in live embryos at earlier stages. In 10-day-old larvae from *chi*/+ outcrosses, we observed abnormal growth of the caudal fin fold in 49% of the progeny (n = 137). In some larvae, the fin grew out more slowly (Fig. 3B), while in others, the fin was curved laterally (Fig. 3C). To confirm their genotype, the larvae were sorted by tail phenotype and raised until they could be identified unambiguously as WT or *chi*/+; in all fish, the early larval phenotype predicted the later phenotype. The

larval phenotype is evident as early as 3 days, when the caudal fins of *chi*/+ larvae are 80% the width of WT fins (data not shown).

We intercrossed *chi*/+ fish to determine whether *chi/chi* progeny display additional or more severe phenotypes. In the first week of development, 72% ($n = 238$) of the larvae displayed the fin growth abnormality described above, but no morphologically distinct class of mutant embryos was observed that might correspond to homozygous mutants. However, approximately one-fourth of the larvae (29%) failed to develop swim bladders or begin feeding, suggesting that *chi* homozygotes have defects in other organ systems.

Molecular identification of chi as colla1

As a first step toward the molecular identification of *chi*, we mapped the mutation through bulked segregant analysis of DNA from haploid WT and mutant embryos (Postlethwait et al., 1994). *chi*/+ females of AB/WIK backgound were used to generate haploid embryos; these were sorted as mutant or wild-type at 5 days based on caudal fin phenotype (Fig. 3A–C), and DNA was prepared from individual embryos. PCR analysis of randomly distributed polymorphic markers on pooled samples of mutant and wild-type DNA demonstrated linkage to LG3 (data not shown). Individual samples were analyzed further to determine the precise map position of *chi* (Fig. 3D and E).

The vast majority of human OI cases are due to a mutation in either *COL1A1* or *COL1A2*, the genes encoding the two chains of type I collagen. Because of the phenotypic similarities of *chi* to human OI, we tested zebrafish *col1a1* and *col1a2* genes as candidates for the *chi* locus. Expressed sequence tags (ESTs) had been isolated representing partial clones of zebrafish genes homologous to both mammalian genes (http://www.genetics.wustl.edu/fish_lab/frank/cgi-bin/fish/). We analyzed expression of both collagen genes by in situ hybridization. In embryos at 1 day, there was substantial overlap in the expression patterns, with both genes expressed strongly in ectoderm (Fig. 4A and B). However, only *col1a1* was expressed at the distal edges of outgrowing fin folds (Fig. 4A), consistent with the larval fin fold defect observed in *chi*/+ and *chi/chi* fish. We further examined *col1a1* expression in developing skeletal elements at later stages. Strong expression was detected at 3 days in the cleithrum (Fig. 4C), one of the first membranous bones to form in zebrafish larvae (Cubbage and Mabee, 1996); in numerous groups of cells surrounding cartilages in the larval skull (Fig. 4E); in the forming vertebral column (Fig. 4D and F); and in the ribs (Fig. 4G).

Northern blot analysis of total RNA from adult WT and *chi*/+ fish did not show either a decrease in *col1a1* expression or an RNA species of a different size (data not shown). All progeny from an intercross of *chi*/+ fish showed the same pattern and level of expression for both collagen genes following in situ hybridization (data not shown). However, greater than two-thirds of mutations causing OI are missense mutations in one of the two type I collagen genes, which do not apparently affect levels of expression (Kuivaniemi et al., 1997). We placed both genes on the zebrafish map (Fig. 3E) using a mouse–zebrafish radiation hybrid mapping panel (Hukriede et al., 1999). The *col1a2* gene mapped to LG19, ruling it out as the *chi* locus. However, *col1a1* localized to the same region of LG3 as *chi*. We identified a polymorphism in *col1a*1 and placed it on the *chi* mapping panel, finding no recombinants with *chi* in 128 individuals.

We used the EST clone to screen for additional *col1a1* cDNA clones, and obtained 3.7 kb of sequence. Later searches of the EST and genomic sequence databases discovered clones containing the 5′ end of the coding sequence; RT-PCR was used to amplify the remaining portion of cDNA. The resulting sequence of zebrafish *col1a1* is highly homologous to the human gene; at the amino acid level, the two proteins are 76% identical (Fig. 5A). In addition, both contain the uninterrupted glycine triplet repeat region (underline in Fig. 5A) characteristic of fibrillar collagens.

RT-PCR products from *chi*/+ adult RNA were sequenced directly to identify missense mutations. The initial sample analyzed was heterozygous at 19 positions; however, 17 of these polymorphisms did not change the encoded amino acids. The polymorphism at position 2617 changes the encoded amino acid from serine to alanine, but was also detected in samples from wild-type fish. At position 2207 of the coding sequence, the *chi*/+ cDNA had both a G, the wild-type sequence, and an A, which is predicted to change the encoded amino acid from glycine to aspartate (Fig. 5B). This sequence change was confirmed by similar analysis of RNA from pools of *chi*/+ and *chi/chi* embryos, and was not observed in samples derived from WT embryos or adults.

As confirmation that the mutation causes the *chi* mutant phenotype, additional WT, *chi*/+, and *chi/chi* embryos, and WT and *chi*/+ adults, were genotyped. The *col1a1* sequence change in *chi* is predicted to introduce a *Bst*F5I restriction site. Either cDNA or genomic DNA samples were subjected to PCR with primers flanking the mutation site, and digested with *Bst*F5I (Fig. 5C). A total of 147 embryos and 59 adults were genotyped, with no recombinants observed between *chi* and the *col1a1* mutation. Together with the results from the *chi* mapping panel, this places *chi* a maximum of 0.3 cM from *col1a1*.

We also genotyped 30 putative homozygous embryos; while most were homozygous for the mutation, 2 proved to be heterozygous. However, the only morphological feature we found to distinguish homozygotes was failure to inflate the swim bladder, which is a nonspecific feature and can occur in WT embryos.

Discussion

Radiography is faster and simpler to perform than standard histological methods for examining skeletal anatomy and provides considerable detail without requiring the sacrifice of the animal. X-rays can also be used as a rapid survey of known mutants of potential interest for skeletal abnormalities. The small size of adult zebrafish and the availability of a convenient, short-acting anesthetic makes it practical to X-ray large numbers of animals efficiently. Thus, radiography is a powerful screening tool for the identification of new mutants affecting skeletal development. In this study, we describe the normal adult skeletal anatomy in the zebrafish with radiography, present the use of radiography to screen for novel mutations, and characterize a zebrafish skeletal mutant as a model for human osteogenesis imperfecta.

Mutational screen for zebrafish skeletal dysplasias

Zebrafish are well-suited to identify early embryonic phenotypes because of the ease with which the transparent embryos can be screened visually for morphological abnormalities. The use of X-rays makes the adult skeleton almost as accessible, facilitating genetic screens for late-acting mutations. We initially chose to focus on the identification of dominant skeletal mutants, for two reasons. Logistically, such a screen requires raising relatively few fish, and mutagenized fish created for other screens can also be examined by X-ray. In addition, many human skeletal dysplasias whose genetics have been described are due to dominant mutations (Ho et al., 2000; McKusick and Amberger, 1993; McKusick and Amberger, 1994), and it seems likely that screening for dominant mutations in zebrafish will identify similar dysplasias. There is little data available to judge the expected frequency of dominant mutations affecting skeletal development or other traits, since they have not been systematically recovered in large-scale zebrafish mutagenesis screens to date. During 1 large screen, 14 dominant mutations were recovered representing 10 complementation groups; they affected easily visible processes, such as pigmentation, size, and fin growth (Haffter et al., 1996b). From the 3857 genomes that were screened, a frequency of approximately 1 visible, dominant mutant was obtained for every 275 genomes. By confining our screen to skeletal phenotypes, we would expect to identify mutants at a somewhat lower frequency, perhaps 1 out of every 500–1000 genomes screened. Out of 2000 genomes screened, we have isolated 1 dominant mutation, consistent with the estimation of expected mutation frequency.

Zebrafish model of osteogenesis imperfecta

The first skeletal mutant we have characterized, *chi*, phenotypically resembles the human skeletal dysplasia OI. Both are dominantly acting mutations, which allow normal cartilage formation but result in a general defect in bone growth. We also observe uneven mineralization of growing bone and fragile bones with frequent fractures in *chi*/+ fish, features characteristic of OI (reviewed in Shapiro et al., 1996).

OI is usually caused by missense mutations in one of the genes encoding type I collagen, the predominant protein component of bone matrix (reviewed in Kuivaniemi et al., 1997). Type I collagen in mammals is a heterotrimer composed of two α1 and one α2 chain, encoded respectively by the *COL1A1* and *COL1A2* genes. Both collagen protein chains contain a long, uninterrupted triplet repeat domain (Gly-X-Y), which is necessary for trimer formation and proper posttranslational processing. The composition of type I collagen has not been demonstrated in zebrafish and may vary among tissues. The observation of high *col1a1* expression in fin folds of larval zebrafish, with undetectable *col1a2* expression in the fin folds, suggests that type I collagen in the larval fin fold may be composed entirely of α1 chains. There may also be additional type I collagen genes, with the exact composition of collagen varying by tissue or developmental stage according to the specific expression patterns of the genes. In the trout, type I collagen comprises three subunits, encoded by the *col1a1*, *col1a2*, and *col1a3* genes (Saito et al., 2001). There is a cluster of EST sequences in the zebrafish EST database (cluster 318870) from a gene most closely related to the trout *col1a3* gene. This cluster has been mapped to a region of LG12 that also shows conserved synteny with the location of human *COL1A1* (Hukriede et al., 2001), suggesting that this gene and *chi* are both orthologues of the mammalian gene produced by gene duplication. Therefore, we propose that *chi* be referred to as *col1a1.1*, and the gene on LG12 as *col1a1.2*.

The *chi* locus maps to the same interval on LG3 as *col1a1*, and strong expression of *col1a1* in the larval fin folds is consistent with the early fin growth defect observed in *chi* mutants. In addition, *col1a1* is expressed strongly in numerous bony skeletal elements during development. The vast majority of mutations in *COL1A1* causing OI (93/161) are amino acid substitutions altering a glycine in the triplet repeat region (http://www.le.ac.uk/genetics/collagen/). The glycine substitutions slow the assembly of the triple helix, allowing the chains to be more extensively hydroxylated. The resulting collagen molecules are poorly incorporated into the larger collagen fibrils; this can have a number of effects, including decreasing the overall amount of bone matrix, decreasing its tensile strength, and interfering with its mineralization (reviewed in Shapiro et al., 1996). Our evidence supports the finding that *chi* is caused by a similar mutation in *col1a1*. The WT zebrafish *col1a1* sequence encodes an uninterrupted Gly-X-Y repeat over the homologous segment to the human gene. However, sequence analysis of *col1a1* from *chi*/+ fish revealed a glycine to

A

```
MFSFVDILLALLLNATVLLARGQ-------GEDDRTGGSCTLDGQVYNDRDVWKPEPCQICVCDSGTVMCDEVICEDTSD  73
MFSFVDLRLLLLLAATALLTHGQEEGQVEGQDEDIPPITCVQNGLRYHDRDVWKPEPCRICVCDNGKVLCDDVICDETKN  80
******. * *** ** **..**      *.* *    .*   *  *.**********.***** * *.**.***..*

CPNPVIAHDECCPVCPD----DDFQEPSVEGPRGSPGDKGERGPANPPGNDGIHEQSVLPVPTSHSG----PAALGGNLS  145
CPGAEVPEGECCPVCPDGSESPTDQETTGVEGPKGDTGPRGPRGPAGPPGRDGIPGQPGLPGPPGPPGPPGPPGLGGNFA  160
**.  .   ********      * .   ****.*  * .* ****.*** ***  *  ** *    *   *  **** .

PQMSGGFDEKSSP-MAVPGPMGPMGPRGAPGPPGPSGPQGFTGPPGEPGEAGAPGPMGPRGAAGPPGKNGEDGESGKPGR  224
PQLSYGYDEKSTGGISVPGPMGPSGPRGLPGPPGAPGPQGFQGPPGEPGEPGASGPMGPRGPPGPPGKNGDDGEAGKPGR  240
**.* *.****.  ..******* **** *****  ***** ******** ** *******  *******.***.*****

PGERGPPGPQGARGFPGTPGLPGIKGHRGFSGLDGAKGDAGPAGPKGEPGAPGENGTPGAMGPRGLPGERGRAGPPGAAG  304
PGERGPPGPQGARGLPGTAGLPGMKGHRGFSGLDGAKGDAGPAGPKGEPGSPGENGAPGQMGPRGLPGERGRPGAPGPAG  320
************** *** ****.*************************.*****.** ************ * ** **

ARGNDGAAGAAGPPGPTGPAGPPGFPGGPGSKGEVGPQGSRGAEGPQGARGEAGNPGPAGPAGPAGNNGADGAPGAKGAP  384
ARGNDGATGAAGPPGPTGPAGPPGFPGAVGAKGEAGPQGPRGSEGPQGVRGEPGPPGPAGAAGPAGNPGADGQPGAKGAN  400
*******.******************  *.*** **** **.***** *** * ***** ****** **** ******

GAPGIAGAPGFPGPRGPPGAAGAAGAPGPKGNTGEAGAPGAKGEAGAKGEAGAQGVQGPPGPPGEEGKRGPRGEPGAGGA  464
GAPGIAGAPGFPGARGPSGPQGPGGPPGPKGNSGEPGAPGSKGDTGAKGEPGPVGVQGPPGPAGEEGKRGARGEPGPTGL  480
************* *** *  *  * ******.** ****.**..***** *  ******** ******* *****  *

RGPTGERGAPGARGFPGADGAAGPRGAPGERGGPGVVGPKGATGEPGRNGEPGMPGSKGMTGSPGSPGPDGKTGPGGAPG  544
PGPPGERGGPGSRGFPGADGVAGPKGPAGERGSPGPAGPKGSPGEAGRPGEAGLPGAKGLTGSPGSPGPDGKTGPPGPAG  560
 ** **** **.******** ***.*  **** **  ****. ** ** ** *.**.**.*************** *  *

QDGRPGPPGPVGARGQPGVMGFPGPKGAAGEAGKPGERGVMGAIGATGAPGKDGDVGAPGAPGPAGPAGERGEQGAAGPP  624
QDGRPGPPGPPGARGQAGVMGFPGPKGAAGEPGKAGERGVPGPPGAVGPAGKDGEAGAQGPPGPAGPAGERGEQGPAGSP  640
********** ***** ************** ** ***** *  ** *  ****. ** * ************** ** *

GFQGLPGPQGATGEPGKSGEQGAPGEAGAPGPSGSRGDRGFPGERGAPGPAGPVGARGSPGSAGNDGAKGESGAAGAPGA  704
GFQGLPGPAGPPGEAGKPGEQGVPGDLGAPGPSGARGERGFPGERGVQGPPGPAGPRGANGAPGNDGAKGDAGAPGAPGS  720
******** *  ** ** **** **. *******.**.********  ** ** * **. *. *******..** ****.

QGPPGLQGMPGERGAAGLPGLKGDRGDQGAKGADGAAGKDGIRGMTGPIGPPGPAGAPGDKGESGAQGLVGPTGARGPPG  784
QGAPGLQGMPGERGAAGLPGPKGDRGDAGPKGADGSPGKDGVRGLTGPIGPPGPAGAPGDKGESGPSGPAGPTGARGAPG  800
** ****************** ****** * *****. ****.**.********************  *  ******* **

ERGETGAPGPAGFAGPPGADGLPGAKGEPGDNGAKGDAGAPGPAGATGAPGPQGPVGATGPKGARGAAGPPGATGFPGAA  864
DRGEPGPPGPAGFAGPPGADGQPGAKGEPGDAGAKGDAGPPGPAGPAGPPGPIGNVGAPGAKGARGSAGPPGATGFPGAA  880
.*** * ************** ********* ******* ***** .* *** * *** * *****.**************

GRVGPPGPSGNSGPPGPPGPAGKEGQKGNRGETGPAGRTGEVGAAGPPGAPGEKGNPGAEGATGPAGIPGPQGIGGQRGI  944
GRVGPPGPSGNAGPPGPPGPAGKEGGKGPRGETGPAGRPGEVGPPGPPGPAGEKGSPGADGPAGAPGTPGPQGIAGQRGV  960
***********.************** ** ********* ****  ****  **** ***.* .*  * ****** ****.

VGLPGQRGERGFPGLPGPSGEIGKQGPSGPSGERGPPGPMGPPGLAGPPGEPGREGTPGNEGSAGRDGAAGPKGDRGETG 1024
VGLPGQRGERGFPGLPGPSGEPGKQGPSGASGERGPPGPMGPPGLAGPPGESGREGAPAAEGSPGRDGSPGAKGDRGETG 1040
********************** ******* ********************** ****.*  *** ****. * *********

PSGTPGAPGPPGAAGPIGPAGKTGDRGETGPAGVPGPAGPSGPRGPSGPAGARGDKGETGEAGERGMKGHRGFTGMPGPP 1104
PAGPPGAPGAPGAPGPVGPAGKSGDRGETGPAGPAGPVGPVGARGPAGPQGPRGDKGETGEQGDRGIKGHRGFSGLQGPP 1120
*.* ***** *** **.*****.**********  ** ** * ***.** * ********* *.**.******.*. ***

GPPGPSGESGPAGASGPAGPRGPAGSAGSAGKDGMSGLPGPIGPPGPRGRNGEIGPAGPPGPPGPPGAPGPSGGGFDIGF 1184
GPPGSPGEQGPSGASGPAGPRGPPGSAGAPGKDGLNGLPGPIGPPGPRGRTGDAGPVGPPGPPGPPGPPGPPSAGFDFSF 1200
****  ** **.*********** ****. ****. ***************.*. ** ********** ***   ***  *

IAQP-QEKAPDPFRHFRADDANVMRDRDLEVDTTLKSLSQQIESIISPDGTKKNPARTCRDLKMCHPDWKSGEYWIDPDQ 1263
LPQPPQEKAHDGGRYYRADDANVVRDRDLEVDTTLKSLSQQIENIRSPEGSRKNPARTCRDLKMCHSDWKSGEYWIDPNQ 1280
. ** **** *  * .*******.******************** * **.*..************** ********** *

GCNQDAIKVYCNMETGETCVNPTESAIPKKNWYTSKNIKEKKHVWFGEAMTDGFQFEYGSEGSKPEDVNIQLTFLRLMST 1343
GCNLDAIKVFCNMETGETCVYPTQPSVAQKNWYISKNPKDKRHVWFGESMTDGFQFEYGGQGSDPADVAIQLTFLRLMST 1360
*** *****.********** **. .. .**** *** *.*.******.********** .** * ** **********

EASQNITYHCKNSIAYMDQASGNLKKALLLQGSNEIEIRAEGNSRFTYSVTEDGCTSHTGAWGKTVIDYKTTKTSRLPII 1423
EASQNITYHCKNSVAYMDQQTGNLKKALLLKGSNEIEIRAEGNSRFTYSVTVDGCTSHTGAWGKTVIEYKTTKSSRLPII 1440
*************.*****  .*********.******************** ***************.*****.******

DIAPMDVGAPNQEFGIEVGPVCFL 1447
DVAPLDVGAPDQEFGFDVGPVCFL 1464
*.**.***** **** .*******
```

Fig. 5. Molecular characterization of *chi* locus. (A) Protein sequence comparison of the zebrafish and human α1 chain of type I collagen; the zebrafish sequence is on top. The triplet repeat region (Gly-X-Y) of both proteins is underlined; the glycine residue substituted in *chi* is indicated with an arrowhead. (B) Sequence change in *colla1* associated with the *chi* mutant phenotype; the sequence traces are shown for WT and *chi*/+ adult RT-PCR products, with a mixture of A and G at position 390 in the *chi*/+ sample. To the right, the cDNA sequences and corresponding amino acid residues are given for WT and *chi*, with the *Bst*F5I site created by the mutation indicated (arrowhead). (C) RNA samples from individual adult fish (left panel) or embryos (right panel) of the indicated genotypes were subjected to RT-PCR as described in materials and methods. Products were run out before (−) or after (+) digestion with *Bst*F5I. All uncut samples were the expected size of 1180 bp (*); however, after digestion, the *chi* sequence was cut into two bands of 382 and 798 bp (arrowheads). The first lane in the left panel shows molecular weight markers (100 bp ladder; Life Technologies).

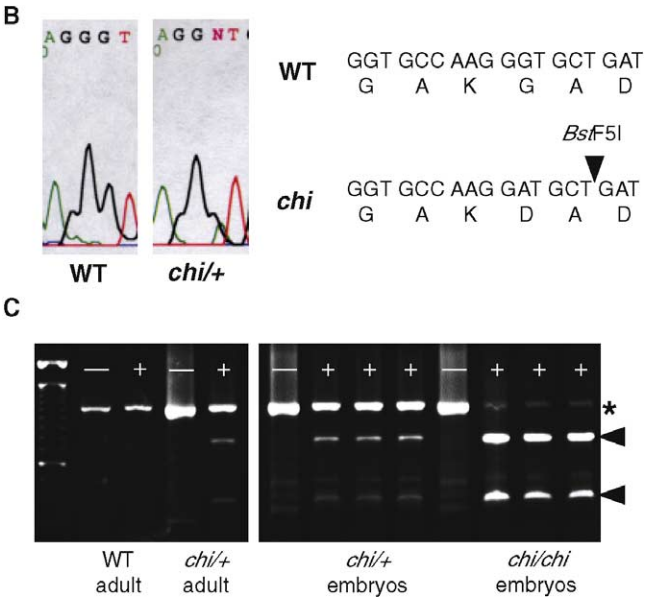

Fig. 5 (*continued*)

aspartate substitution, interrupting the otherwise conserved triplet repeat domain. In addition, analysis of bone in *chi*/+ fish by electron microscopy has revealed defects in the collagenous matrix and accumulation of collagen fibrils in the endoplasmic reticulum of osteoblasts, both findings observed in OI tissue (data not shown).

The characterization of the *chi* molecular defect confirms the similarity of the collagen assembly process and the importance of type I collagen in bone formation in zebrafish. The similarities between OI and the *chi* mutant phenotype also validate the zebrafish as a model for bone growth in humans. Several mouse models exist for OI (Chipman et al., 1993; Harbers et al., 1984; Khillan et al., 1991; Pereira et al., 1993; Sillence et al., 1993), including most recently a model made with knock-in technology to mimic the missense mutations usually found in human OI (Forlino et al., 1999). The *chi* mutant also appears to be an accurate model both molecularly and phenotypically for the majority of OI cases, with the heterozygotes viable but displaying severe disturbances in bone growth. Easy access to zebrafish embryos and larvae, and the availability of specific markers for stages of bone development, will allow detailed examination of the early steps in bone formation in *chi* mutants. In addition, the processes of fin growth and regeneration in zebrafish offer excellent models for bone growth and repair, in a tissue that is easily accessible and can be sampled repeatedly.

Radiography is a powerful technique to detect subtle abnormalities in the adult zebrafish skeleton. Using X-rays, we have screened for skeletal mutants in adult zebrafish and isolated a dominant mutation causing a skeletal dysplasia analogous to human OI. Many powerful genetic and embryological methods already exist for the zebrafish, as well as large collections of identified mutants. The adaptation of existing techniques such as radiography will extend the usefulness of zebrafish as a genetic system to study the regulation of skeletal patterning and development.

Acknowledgments

We thank Mary Mullins for allowing us to X-ray ENU-mutagenized fish in her facility, and Steve Johnson for the gift of an adult fin cDNA library. We thank Paula Mabee for advice on the identities of bones in radiographs. This work was supported in part by a Clinical Investigator Development Award from NINDS (NS01851), a Seed Grant from the Osteogenesis Imperfecta Foundation, and NIH Grant AR48101 (to S.F.), a Pew Scholar Award (to M.E.H.), and NIH Grants GM53373 and HL63792 (to P.J.).

References

Bonadio, J., Saunders, T.L., Tsai, E., Goldstein, S.A., Morris-Wiman, J., Brinkley, L., Dolan, D.F., Altschuler, R.A., Hawkins, J.E.J., Bateman, J.F., et al., 1990. Transgenic mouse model of the mild dominant form of osteogenesis imperfecta. Proc. Natl. Acad. Sci. USA 87, 7145–7149.

Brunet, L.J., McMahon, J.A., McMahon, A.P., Harland, R.M., 1998. Noggin, cartilage morphogenesis, and joint formation in the mammalian skeleton. Science 280, 1455–1457.

Chipman, S.D., Sweet, H.O., McBride, D.J.J., Davisson, M.T., Marks, S.C.J., Shuldiner, A.R., Wenstrup, R.J., Rowe, D.W., Shapiro, J.R., 1993. Defective pro alpha 2(I) collagen synthesis in a recessive mutation in mice: a model of human osteogenesis imperfecta. Proc. Natl. Acad. Sci. USA 90, 1701–1705.

Cubbage, C.C., Mabee, P.M., 1996. Development of the cranium and paired fins in the zebrafish *Danio rerio* (Osariophysi, Cyprinidae). J. Morphcol. 229, 121–160.

Driever, W., Solnica-Krezel, L., Schier, A.F., Neuhauss, S.C., Malicki, J., Stemple, D.L., Stainier, D.Y., Zwartkruis, F., Abdelilah, S., Rangini, Z., et al., 1996. A genetic screen for mutations affecting embryogenesis in zebrafish. Development 123, 37–46.

Dunn, N.R., Winnier, G.E., Hargett, L.K., Schrick, J.J., Fogo, A.B., Hogan, B.L., 1997. Haploinsufficient phenotypes in Bmp4 heterozygous null mice and modification by mutations in Gli3 and Alx4. Dev. Biol. 188, 235–247.

el Ghouzzi, V., Le Merrer, M., Perrin-Schmitt, F., Lajeunie, E., Benit, P., Renier, D., Bourgeois, P., Bolcato-Bellemin, A.L., Munnich, A., Bonaventure, J., 1997. Mutations of the *TWIST* gene in the Saethre-Chotzen syndrome. Nat. Genet. 15, 42–46.

Fisher, S., Amacher, S.L., Halpern, M.E., 1997. Loss of cerebum function ventralizes the zebrafish embryo. Development 124, 1301–1311.

Fisher, S., Halpern, M.E., 1999. Patterning the zebrafish axial skeleton requires early *chordin* function. Nat. Genet. 23, 442–446.

Forlino, A., Porter, F.D., Lee, E.J., Westphal, H., Marini, J.C., 1999. Use of the Cre/lox recombination system to develop a non-lethal knock-in murine model for osteogenesis imperfecta with an alpha1(I) G349C substitution. Variability in phenotype in BrtlIV mice. J. Biol. Chem. 274, 37923–37931.

Francomano, C.A., McIntosh, I., Wilkin, D.J., 1996. Bone dysplasias in man: molecular insights. Curr. Opin. Genet. Dev. 6, 301–308.

Gong, Y., Krakow, D., Marcelino, J., Wilkin, D., Chitayat, D., Babul-Hirji, R., Hudgins, L., Cremers, C.W., Cremers, F.P., Brunner, H.G., et al.,

1999. Heterozygous mutations in the gene encoding noggin affect human joint morphogenesis. Nat. Genet. 21, 302–304.

Haffter, P., Granato, M., Brand, M., Mullins, M.C., Hammerschmidt, M., Kane, D.A., Odenthal, J., van Eeden, F.J., Jiang, Y.J., Heisenberg, C.P., et al., 1996a. The identification of genes with unique and essential functions in the development of the zebrafish, *Danio rerio*. Development 123, 1–36.

Haffter, P., Odenthal, J., Mullins, M.C., Lin, S., Farrell, M.J., Vogelsang, E., Haas, F., Brand, M., van Eeden, F.J.M., Furutani-Seiki, M., et al., 1996b. Mutations affecting pigmentation and shape of the adult zebrafish. Dev. Genes Evol. 206, 260–276.

Harbers, K., Kuehn, M., Delius, H., Jaenisch, R., 1984. Insertion of retrovirus into the first intron of alpha 1(I) collagen gene to embryonic lethal mutation in mice. Proc. Natl. Acad. Sci. USA 81, 1504–1508.

Ho, N., Jia, L., Driscoll, C., Gutter, E., Francomano, C., 2000. A skeletal gene database. J. Bone Mineral Res. 15, 2095–2122.

Hrabe de Angelis, M.H., Flaswinkel, H., Fuchs, H., Rathkolb, B., Soewarto, D., Marschall, S., Heffner, S., Pargent, W., Wuensch, K., Jung, M., et al., 2000. Genome-wide, large-scale production of mutant mice by ENU mutagenesis. Nat. Genet. 25, 444–447.

Hukriede, N.A., Joly, L., Tsang, M., Miles, J., Tellis, P., Epstein, J.A., Barbazuk, W.B., Li, F.N., Paw, B., Postlethwait, J.H., et al., 1999. Radiation hybrid mapping of the zebrafish genome. Proc. Natl. Acad. Sci. USA 96, 9745–9750.

Hukriede, N., Fisher, D., Epstein, J., Joly, L., Tellis, P., Zhou, Y., Barbazuk, B., Cox, K., Fenton-Noriega, L., Hersey, C., et al., 2001. The LN54 radiation hybrid map of zebrafish expressed sequences. Genome Res. 11, 2127–2132.

Jabs, E.W., Muller, U., Li, X., Ma, L., Luo, W., Haworth, I.S., Klisak, I., Sparkes, R., Warman, M.L., Mulliken, J.B., et al., 1993. A mutation in the homeodomain of the human MSX2 gene in a family affected with autosomal dominant craniosynostosis. Cell 75, 443–450.

Khillan, J.S., Olsen, A.S., Kontusaari, S., Sokolov, B., Prockop, D.J., 1991. Transgenic mice that express a mini-gene version of the human gene for type I procollagen (COL1A1) develop a phenotype resembling a lethal form of osteogenesis imperfecta. J. Biol. Chem. 266, 23373–23379.

Knapik, E.W., Goodman, A., Atkinson, O.S., Roberts, C.T., Shiozawa, M., Sim, C.U., Weksler-Zangen, S., Trolliet, M.R., Futrell, C., Innes, B.A., et al., 1996. A reference cross DNA panel for zebrafish (*Danio rerio*) anchored with simple sequence length polymorphisms. Development 123, 451–460.

Komori, T., Yagi, H., Nomura, S., Yamaguchi, A., Sasaki, K., Deguchi, K., Shimizu, Y., Bronson, R.T., Gao, Y.H., Inada, M., et al., 1997. Targeted disruption of Cbfa1 results in a complete lack of bone formation owing to maturational arrest of osteoblasts. Cell 89, 755–764.

Kuivaniemi, H., Tromp, G., Prockop, D.J., 1997. Mutations in fibrillar collagens (types I, II, III, and XI), fibril-associated collagen (type IX), and network-forming collagen (type X) cause a spectrum of diseases of bone, cartilage, and blood vessels. Hum. Mutat. 9, 300–315.

Lee, B., Thirunavukkarasu, K., Zhou, L., Pastore, L., Baldini, A., Hecht, J., Geoffroy, V., Ducy, P., Karsenty, G., 1997. Missense mutations abolishing DNA binding of the osteoblast-specific transcription factor OSF2/CBFA1 in cleidocranial dysplasia. Nat. Genet. 16, 307–310.

Li, Q.Y., Newbury-Ecob, R.A., Terrett, J.A., Wilson, D.I., Curtis, A.R., Yi, C.H., Gebuhr, T., Bullen, P.J., Robson, S.C., Strachan, T., et al., 1997. Holt-Oram syndrome is caused by mutations in TBX5, a member of the Brachyury (T) gene family. Nat. Genet. 15, 21–29.

McKusick, V.A., Amberger, J.S., 1993. The morbid anatomy of the human genome: chromosomal location of mutations causing disease. J. Med. Genet. 30, 1–26.

McKusick, V.A., Amberger, J.S., 1994. The morbid anatomy of the human genome: chromosomal location of mutations causing disease (update 1 December 1993). J. Med. Genet. 31, 265–279.

Morin-Kensicki, E.M., Eisen, J.S., 1997. Sclerotome development and peripheral nervous system segmentation in embryonic zebrafish. Development 124, 159–167.

Morin-Kensicki, E.M., Melancon, E., Eisen, J.S., 2002. Segmental relationship between somites and vertebral column in zebrafish. Development 129, 3851–3860.

Mullins, M.C., Hammerschmidt, M., Haffter, P., Nüsslein-Volhard, C., 1994. Large-scale mutagenesis in the zebrafish: in search of genes controlling development in a vertebrate. Curr. Biol. 4, 189–202.

Mundlos, S., Otto, F., Mundlos, C., Mulliken, J.B., Aylsworth, A.S., Albright, S., Lindhout, D., Cole, W.G., Henn, W., Knoll, J.H., et al., 1997. Mutations involving the transcription factor CBFA1 cause cleidocranial dysplasia. Cell 89, 773–779.

Neuhauss, S.C., Solnica-Krezel, L., Schier, A.F., Zwartkruis, F., Stemple, D.L., Malicki, J., Abdelilah, S., Stainier, D.Y., Driever, W., 1996. Mutations affecting craniofacial development in zebrafish. Development 123, 357–367.

Nolan, P.M., Peters, J., Strivens, M., Rogers, D., Hagan, J., Spurr, N., Gray, I.C., Vizor, L., Brooker, D., Whitehill, E., et al., 2000. A systematic, genome-wide, phenotype-driven mutagenesis programme for gene function studies in the mouse. Nat. Genet. 25, 440–443.

Otto, F., Thornell, A.P., Crompton, T., Denzel, A., Gilmour, K.C., Rosewell, I.R., Stamp, G.W., Beddington, R.S., Mundlos, S., Olsen, B.R., et al., 1997. Cbfa1, a candidate gene for cleidocranial dysplasia syndrome, is essential for osteoblast differentiation and bone development. Cell 89, 765–771.

Pereira, R., Khillan, J.S., Helminen, H.J., Hume, E.L., Prockop, D.J., 1993. Transgenic mice expressing a partially deleted gene for type I procollagen (COLIA1). A breeding line with a phenotype of spontaneous fractures and decreased bone collagen and mineral. J. Clin. Invest. 91, 709–716.

Piotrowski, T., Schilling, T.F., Brand, M., Jiang, Y.J., Heisenberg, C.P., Beuchle, D., Grandel, H., van Eeden, F.J., Furutani-Seiki, M., Granato, M., et al., 1996. Jaw and branchial arch mutants in zebrafish II: anterior arches and cartilage differentiation. Development 123, 345–356.

Postlethwait, J.H., Johnson, S.L., Midson, C.N., Talbot, W.S., Gates, M., Ballinger, E.W., Africa, D., Andrews, R., Carl, T., Eisen, J.S., et al., 1994. A genetic linkage map for the zebrafish. Science 264, 699–703.

Saito, M., Takenouchi, Y., Kunisaki, N., Kimura, S., 2001. Complete primary structure of rainbow trout type I collagen consisting of alpha1(I)alpha2(I)alpha3(I) heterotrimers. Eur. J. Biochem. 268, 2817–2827.

Satokata, I., Maas, R., 1994. Msx1 deficient mice exhibit cleft palate and abnormalities of craniofacial and tooth development. Nat. Genet. 6, 348–356.

Schilling, T.F., 1997. Genetic analysis of craniofacial development in the vertebrate embryo. Bioessays 19, 459–468.

Schilling, T.F., Kimmel, C.B., 1994. Segment and cell type lineage restrictions during pharyngeal arch development in the zebrafish embryo. Development 120, 483–494.

Schilling, T.F., Piotrowski, T., Grandel, H., Brand, M., Heisenberg, C.P., Jiang, Y.J., Beuchle, D., Hammerschmidt, M., Kane, D.A., Mullins, M.C., et al., 1996. Jaw and branchial arch mutants in zebrafish I: branchial arches. Development 123, 329–344.

Shapiro, J.R., Primorac, D., Rowe, D.W., 1996. Osteogenesis imperfecta: current concepts, in: Belizikian, J.P., Raisz, L.G., Rodan, G.A. (Eds.), Principles of Bone Biology, Academic Press, San Diego, pp. 889–902.

Sillence, D.O., Ritchie, H.E., Dibbayawan, T., Eteson, D., Brown, K., 1993. Fragilitas ossium (fro/fro) in the mouse: a model for a recessively inherited type of osteogenesis imperfecta. Am. J. Med. Genet. 45, 276–283.

Streisinger, G., Walker, C., Dower, N., Knauber, D., Singer, F., 1981. Production of clones of homozygous diploid zebra fish (*Brachydanio rerio*). Nature 291, 293–296.

Vajo, Z., Francomano, C.A., Wilkin, D.J., 2000. The molecular and genetic basis of fibroblast growth factor receptor 3 disorders: the achondroplasia family of skeletal dysplasias, Muenke craniosynostosis, and Crouzon syndrome with acanthosis nigricans. Endocr. Rev. 21, 23–39.

van der Hoeven, F., Sordino, P., Fraudeau, N., Izpisua-Belmonte, J.C., Duboule, D., 1996. Teleost HoxD and HoxA genes: comparison with tetrapods and functional evolution of the HOXD complex. Mech. Dev. 54, 9–21.

van Eeden, F.J., Granato, M., Schach, U., Brand, M., Furutani-Seiki, M., Haffter, P., Hammerschmidt, M., Heisenberg, C.P., Jiang, Y.J., Kane, D.A., et al., 1996. Mutations affecting somite formation and patterning in the zebrafish, *Danio rerio*. Development 123, 153–164.

Westerfield, M. (Ed.), 1995. The Zebrafish Book. University of Oregon Press, Eugene, OR.

Wozney, J.M., Rosen, V., Celeste, A.J., Mitsock, L.M., Whitters, M.J., Kriz, R.W., Hewick, R.M., Wang, E.A., 1988. Novel regulators of bone formation: molecular clones and activities. Science 242, 1528–1534.